Journal of ASTM International, Mar. 2004, Vol. 1, No. 3
Paper ID JAI11907
Available online at www.astm.org

Leishan Chen,[1] Bhavani V. Sankar,[2] and Peter G. Ifju[3]

Application of Moire Interferometry for Mode II Testing of Stitched Composites

ABSTRACT: In this paper, two experimental approaches were used to quantify the Mode II fracture toughness of stitched composites. In the End Notched Flexure (ENF) test, which is the traditional Mode II test, the delamination does not open, but slides. This makes it difficult to locate the crack-tip as the crack propagates and hence to estimate the length of crack propagation. This uncertainty introduces significant errors in the estimated value of Mode II fracture toughness, especially of stitched composite laminates. In the present study high sensitive moiré interferometry was used to obtain the full-field displacements as well as the crack tip location in ENF specimens. By using linear elastic fracture mechanics for orthotropic materials, the stress intensity factor can be determined from the relative crack surface displacements behind the crack tip. The results from the displacement matching method are compared with the conventional area method for calculating fracture toughness. It is found that stitching can increase the Mode II fracture toughness of laminated composites by a factor of 2 to 3 depending on the stitch density.

KEYWORDS: ENF test, graphite/epoxy, Mode II fracture toughness, Mode II stress intensity factor, moiré interferometry, stitched laminated composites, translaminar reinforcements

Introduction

The advantages of advanced composites made of continuous fibers in polymer matrices have been well established over the past 20 years. However, there are two major factors that limit the use of these materials: cost of manufacturing and poor through-the-thickness properties. Recent developments in textile technology and composite processing techniques seem to be promising in overcoming the first difficulty. Laminated composites usually exhibit poor interlaminar strength as well as fracture toughness, and hence easily delaminate. There are many methods to improve the out-of-plane properties. Through-the-thickness stitching (Fig. 1) is one of the ideal ways to reinforce the laminates in the thickness direction without significantly deteriorating the in-plane properties [1]. Chen et al. [2, 3] developed experimental methods for determining the Mode I fracture toughness of heavily stitched laminates. Sharma and Sankar [4, 5] studied the Mode II fracture of stitched laminates using ENF specimens. They reported difficulties in locating the crack tip as the delamination propagated with increasing loads. They used the reduction in flexural stiffness of the specimen to estimate the length of delamination. End Notched Flexure (ENF) test has been found to be the most convenient method for determining Mode II fracture toughness of laminated composites and it has been implemented by various researchers [6–12].

[1] Post Doctoral Research Associate, -Department of Mechanical & Aerospace Engineering, PO Box 116250, University of Florida, Gainesville, FL 32611.

[2]Professor, Department of Mechanical & Aerospace Engineering, PO Box 116250, University of Florida, Gainesville, FL 32611.

[3] Associate Professor, Department of Mechanical & Aerospace Engineering, PO Box 116250, University of Flroida, Gainesville, FL 32611.

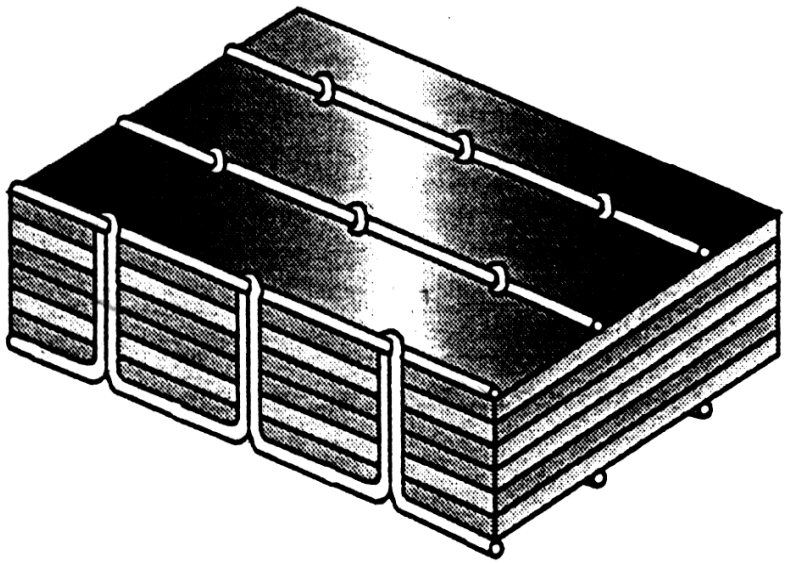

FIG. 1—*Stitched laminated composite.*

To fully understand the complex behavior of laminated composites with translaminar reinforcements, full-field experimental displacement analysis was performed on the microstructural scale of the materials tested in this study. To accomplish this, moiré interferometry [13] was used to document the mechanism of translaminar reinforcement, and their effects on damage tolerance. Moiré interferometry is a laser-based optical experimental stress analysis method that is capable of revealing displacements on the subwavelength scale. The moiré interferometry technique is characterized by high spatial resolution, full-field information, and ability to determine both normal and shear strains. In our setup, the virtual reference grating is 60,960 lines/in (2,400 lines/mm) and the sensitivity is 2.4 fringes/μm displacement. By measuring the relative difference of the fringe orders between two points, the relative movement or slip between two crack surfaces can be determined precisely. By plotting the displacement difference along the entire wake, the effect of stitching on the crack displacement field could be understood. Because moiré interferometry has very high spatial resolution, the location of the crack tip can be determined very accurately.

In the present study, results from linear elastic fracture mechanics of orthotropic materials are used to calculate the stress intensity factor from the relative crack surface displacements. The method can be used to determine the parent or intrinsic fracture toughness of the composite material system and the effective fracture toughness of the stitched composites. The results indicate that stitching can increase Mode II fracture toughness by a factor of 2 to 3 depending on the stitch density.

End-Notched Flexure Test

Two ENF test setups, namely, three-point bending setup and cantilever beam setup, were used to determine the Mode II fracture toughness of stitched composites.

Figure 2 shows the standard ENF Mode II test setup. The specimens were made of AS4-3501 graphite/epoxy system and fabricated with a Teflon layer at the mid-plane to simulate an initial crack. A grating (30480 lines/in or 1200 lines/mm), required for moiré interferometry, was replicated on the edge of the composite specimen. The specimens were cut from a panel which was made from 4 stacks of graphite/epoxy prepreg. Each stack has 7 plies which are oriented at $[45^0/-45^0/0^0/90^0/0^0/-45^0/45^0]$ and the delamination happened at a $45^0/45^0$ interface. The specimens with two different stitch densities, 40 stitches/in^2 (6.2 stitches/cm^2) and 20 stitches/in^2 (3.1 stitches/cm^2) were obtained from the two stitched panels. The spacing between two adjacent rows of stitches was 0.2 inch (0.51 cm) for both densities. The specimen was 5 inches (12.7 cm) long, 1 inch (2.54 cm) wide and 0.23 inch (0.59 cm) thick. The span between the supports was 4 inches (10.2 cm) and the initial crack length, or the distance from the near support to the crack tip, was 1 inch (2.54 cm).

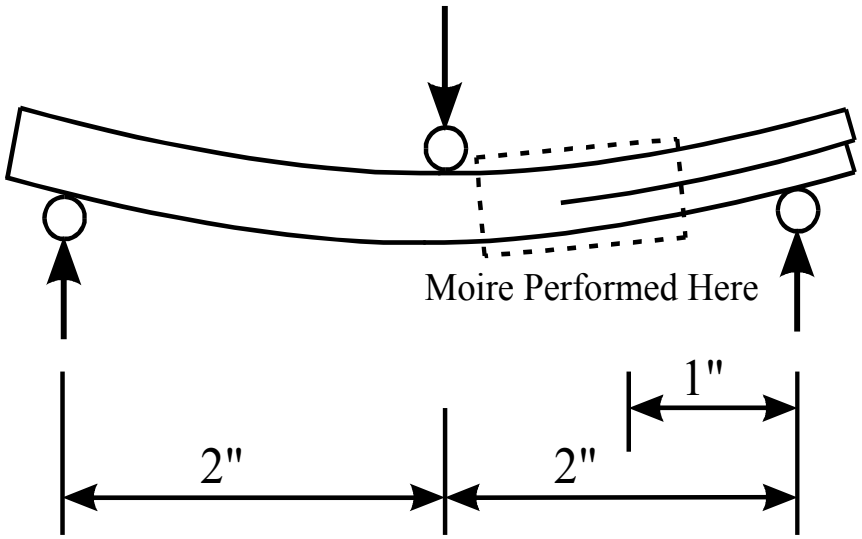

FIG. 2—*Schematic of three-point bending set-up for end notched flexure tests.*

The disadvantage of the three-point bending setup is the limitation of length available for crack propagation. The maximum crack propagation length was around 1 inch (2.54 cm); therefore, it was not possible to obtain a fully developed bridging zone. To fully understand the effect of stitches, the crack should be allowed to propagate as long as possible. The farther the crack propagates, the more the stitches become involved. To accomplish this, a new test setup has been developed as shown in Fig. 3. Using this setup, one can obtain more than 2 inches (5.1 cm) of the crack extension, which is equivalent up to 16 rows of stitches. The length of a specimen for this setup was 7 inches (17.8 cm). Due to large rotation and deflection of the specimen, it is very difficult to apply a high sensitivity moiré interferometry technique for this setup. Because the sensitivity of the moiré interferometry technique is so high, large rotation and deflection will cause the fringe pattern to become too dense to photograph. After trial and error, it was found that to successfully run this test, a PEM-I (portable experimental moiré interferometer) should have at least three adjustments: (1) it should be able to rotate up to 13 º to compensate for the rotation of a specimen (some areas of the specimen can rotate as many as 12 º

during the test); (2) it should be able to move up nearly 1 inch (2.54 cm) to make sure the two laser beams cover the intended area after a specimen is deformed (two overlapped beams are needed to cause interference); and (3) it should be able to move forward and backward at least 2.5 cm (1 inch) to trace the crack tip after crack propagation.

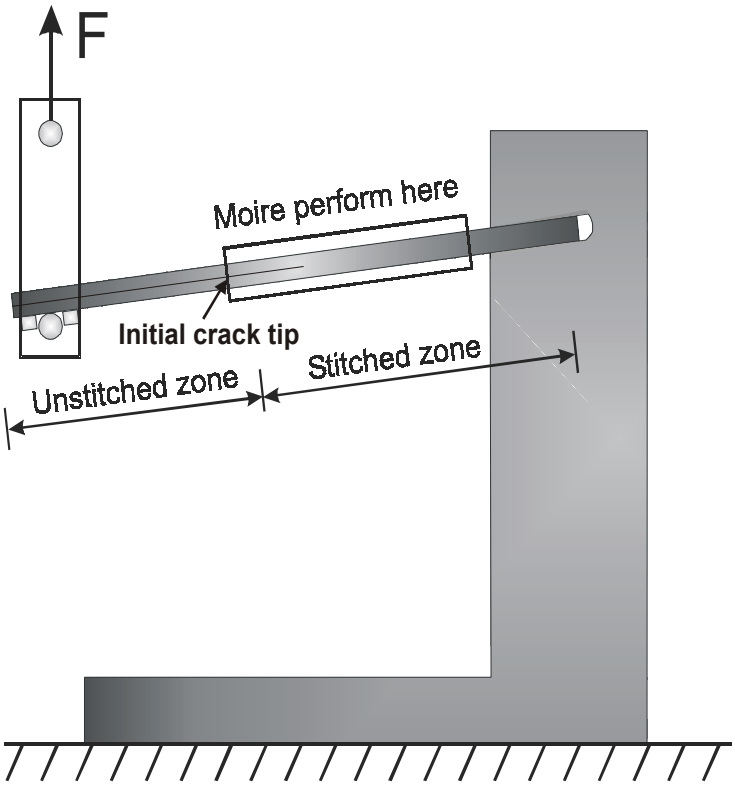

FIG. 3—*Schematic of the cantilever beam setup.*

Methods of Analysis and Results

Two different methods were used to estimate the Mode II fracture toughness from the experimental results. The first one is the area method used in conjunction with ENF tests, which yields the average Mode II critical energy release rate. The second method is based on the crack surface displacements measured using high sensitivity moiré interferometry. While the area method gives the average G_{IIC} over the length of crack propagation, the moiré method results in K_{IIC} (G_{IIC}) at a given crack extension.

Average Strain Energy Release Rate Using Area Method

From the moiré patterns, one can accurately document the full displacement field around the crack tip as well as the exact location of the crack tip, which is the key to determine the crack extension accurately. The area method to obtain the average Mode II fracture toughness is to calculate the area under the load displacement diagram and then use the equation

$$G_{IIc} = \frac{\Delta U}{\Delta A} \tag{1}$$

where ΔU is the total energy for crack propagation determined from the load-deflection diagram and ΔA is the crack area created.

Two diagrams of the load vs. displacement of the three point bending setup are shown in Fig. 4.

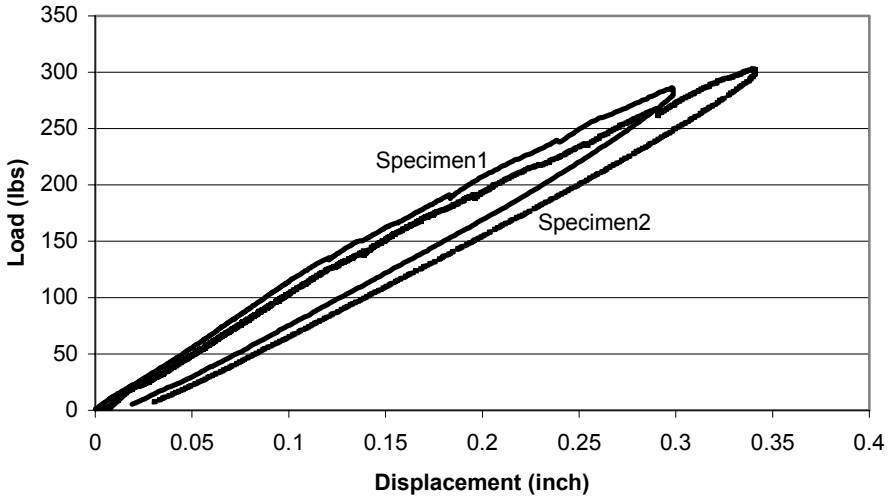

FIG. 4—*Load vs. displacement diagram for the three-point bending setup.*

One can see when the load reached about 111 lbs (489 N), the slopes of the curves started to decrease indicating that the crack began to propagate. Due to crack propagation, the flexural rigidity of the specimens gradually reduces. After the load reached about 300 lbs (1334 N), the specimens were unloaded and the unloading curves were obtained. The area between loading and unloading curves represents the total energy for crack propagation.

Figure 5 shows the load vs. displacement diagram by using the cantilever beam setup. The displacement diagrams of these two specimens match well. When the load reached about 40 lbs (178 N), the crack started to propagate for both specimens and the slopes of the curves began to gradually decrease.

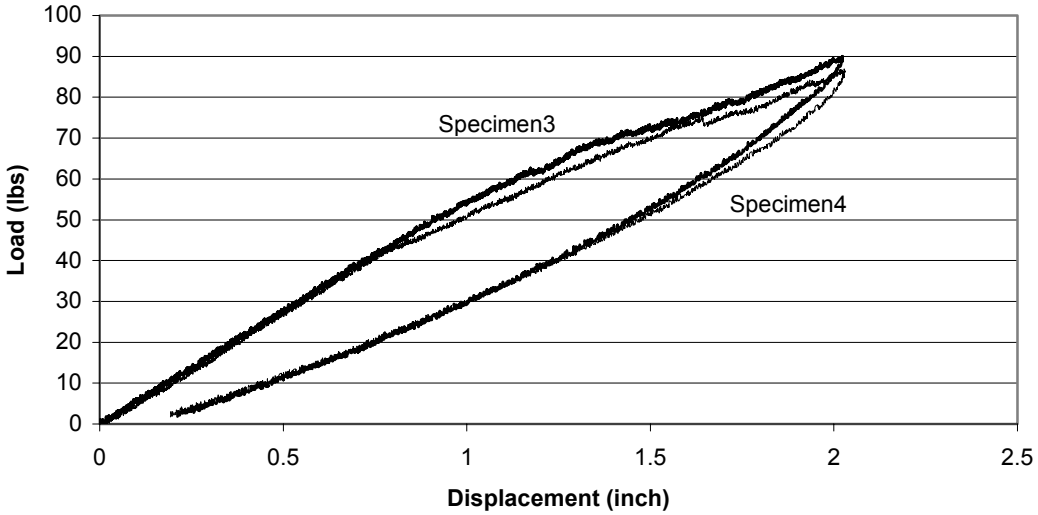

FIG. 5.—*Load vs. displacement diagram for the cantilever beam setup*

This cantilever beam setup gave us much longer final crack lengths than that of the three-point bending setup and the maximum crack lengths of the specimens varied from 1.75 to 2.75 inches (4.5 to 7.0 cm). It is possible to obtain a fully developed bridging zone by using the cantilever beam setup and the maximum value of the effective Mode II fracture toughness ($G_{II\text{-}eff}$) can be obtained accordingly.

Figure 6 presents the comparison of average critical stain energy release rates from the two different setups. The stitching density of the specimens tested by both setups was 20 stitches/in^2 (3.1 stitches/cm^2). The G_{IIC} of specimens 1 and 2 using the three point bending setup is slightly lower than the G_{IIC} of specimens 3, 4 and 5 using the cantilever beam setup. The reason is that the maximum crack extensions of specimens from the three point bending setup are much smaller than the ones from the cantilever beam setup. The more stitches involved, the more energy needed to cause crack propagation. In the cantilever beam setup, the crack was allowed to propagate longer, yielding a longer bridging zone, thus allowing stitches to act to their full potential.

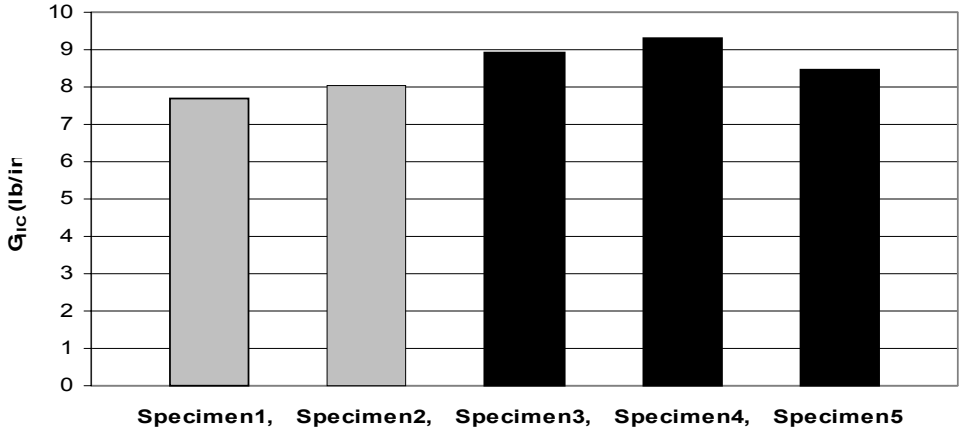

FIG. 6—*Comparison of fracture toughness G_{IIC}. Specimens 1 and 2 were tested by using the three-point bending setup, and specimens 3 through 5 by cantilever beam setup. Stitch density = 20 stitches/in^2 (3.1 stitches /cm^2).*

The G_{IIC} of unstitched specimen was measured in a previous study [5] and was found to be around 3.4 lb/in (600 N/m). From the results presented in Fig. 6, one can note that stitching can increase G_{IIC} by a factor of 2.5 to 3.

Determining the Stress Intensity Factor by Using High Sensitivity Moire Interferometry Technique

Using the area method, one can only obtain the "average G_{IIC}". The G_{IIC} should show variations along the interface because the reinforcement due to stitching is not uniformly distributed. To calculate the G_{IIC} at a given crack length, one needs to measure the crack extension as well as the load precisely. Due to stable crack propagation, the load can be read from the computer attached to the load cell at any instant. Then this load was held constant and the picture of the fringe pattern was taken. From the moiré pattern, the exact location of the crack tip can be determined and hence the crack extension can be measured precisely.

Stress intensity factor for orthotropic brittle materials

For orthotropic materials under plane stress or plane strain conditions, the relationship between stresses and strains can be expressed as

$$\varepsilon_x = a_{11}\sigma_x + a_{12}\sigma_y + a_{16}\tau_{xy}$$

$$\varepsilon_y = a_{12}\sigma_x + a_{22}\sigma_y + a_{26}\tau_{xy} \qquad (2)$$

$$\lambda_{xy} = a_{16}\sigma_x + a_{26}\sigma_y + a_{66}\tau_{xy}$$

The crack-tip stress field for pure Mode II condition is given by [14]

$$\sigma_x = \frac{K_{II}}{\sqrt{2\pi r}} \mathrm{Re}[\frac{1}{s_1 - s_2}(\frac{{s_2}^2}{\sqrt{\cos\theta + s_2 \sin\theta}} - \frac{{s_1}^2}{\sqrt{\cos\theta + s_1 \sin\theta}})] \quad (3a)$$

$$\sigma_y = \frac{K_{II}}{\sqrt{2\pi r}} \mathrm{Re}[\frac{1}{s_1 - s_2}(\frac{1}{\sqrt{\cos\theta + s_2 \sin\theta}} - \frac{1}{\sqrt{\cos\theta + s_1 \sin\theta}})] \quad (3b)$$

$$\tau_{xy} = \frac{K_{II}}{\sqrt{2\pi r}} \mathrm{Re}[\frac{1}{s_1 - s_2}(\frac{s_1}{\sqrt{\cos\theta + s_2 \sin\theta}} - \frac{s_2}{\sqrt{\cos\theta + s_1 \sin\theta}})] \quad (3c)$$

$$u_x = K_{II}\sqrt{\frac{2r}{\pi}}\,\mathrm{Re}\{\frac{1}{s_1 - s_2}[(a_{11}{s_2}^2 + a_{12} - a_{16}s_2)\sqrt{\cos\theta + s_2 \sin\theta} - (a_{11}{s_1}^2 + a_{12} - a_{16}s_1)\sqrt{\cos\theta + s_1 \sin\theta}]\} \quad (3d)$$

$$u_y = K_{II}\sqrt{\frac{2r}{\pi}}\,\mathrm{Re}\{\frac{1}{s_1 - s_2}[(\frac{a_{12}{s_2}^2 + a_{22} - a_{26}s_2}{s_2})\sqrt{\cos\theta + s_2 \sin\theta} - \frac{a_{12}{s_1}^2 + a_{22} - a_{26}s_1}{s_1})\sqrt{\cos\theta + s_1 \sin\theta}]\} \quad (3e)$$

Where s_1, s_2 are function of the material properties as explained in the Appendix.
The relationship between G_{II} and K_{II} for the orthotropic materials is:

$$G_{II} = {K_{II}}^2 \frac{a_{11}}{\sqrt{2}}\sqrt{(\frac{a_{22}}{a_{11}})^{1/2} + \frac{2a_{12} + a_{66}}{2a_{11}}} \quad (4)$$

Results from moiré fringe patterns

Figure 7 shows a series of moiré patterns under various loading conditions by using the three-point bending setup. The stitching density of the tested specimens is 40 stitches/in^2 (6.2 stitches/cm^2) in this setup. These moiré fringe patterns give the full displacement fields. The relative displacement along the horizontal direction can be obtained from the U field while the relative displacement along the vertical direction can be obtained from the V field. The full field of shear strain distribution can be obtained from both U and V fields. As the strain is proportional to the gradient of the fringe pattern, the closer the distance to the crack tip, the denser the fringe pattern is. The location of the crack tip can be determined accurately from the discontinuity in the fringe pattern.

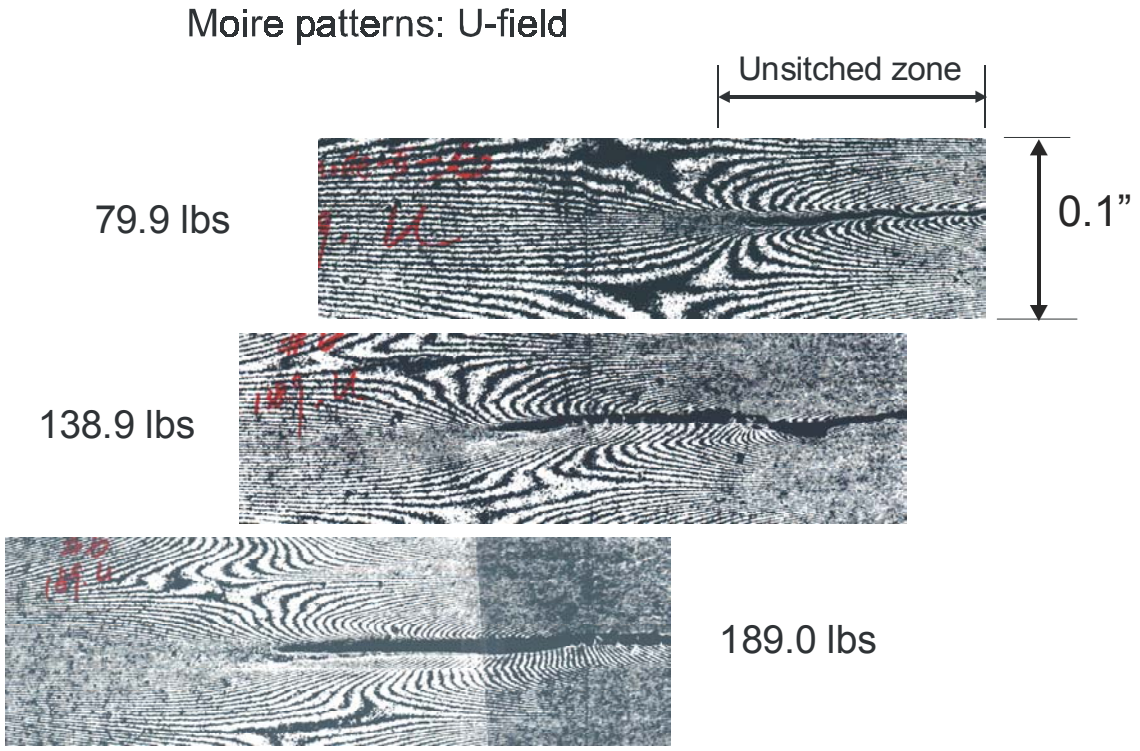

FIG. 7—*Crack tip location corresponding to different loads in the three-point bending setup.*

In order to locate the exact position of the crack tip, a reference line was drawn on the grating by a sharp blade. This line is located inside of the stitched zone and is close to the position that separates the stitched region from the un-stitched region. One can note from Fig. 7 that when the load was 79.9 lbs (355 N), the crack tip was behind the reference line and the crack is still in the unstitched zone. As the load reached 138.9 lbs (618 N), the crack tip was ahead of the reference line and the crack propagated into the stitched zone. When the load reached 189.0 lbs (840 N), the crack tip was far ahead of the reference line, and the crack had passed through numerous stitches.

Fringe patterns from the cantilever beam setup are shown in Fig. 8. The specimens with the stitching density of 20 stitches/in^2 (3.1 stitches/cm^2) were used in this setup. The reference line is right on the position that separates the stitched zone from the un-stitched zone. The stitched zone is ahead of the reference line and unstitched zone is behind the line. The crack tip was behind the reference line when the load was (31.6 lbs) (140 N) and crack tip was right on the line as the load reached 39.7 lbs (176 N) -- that means 39.7 lbs (176 N) was the initial critical load for this specimen.

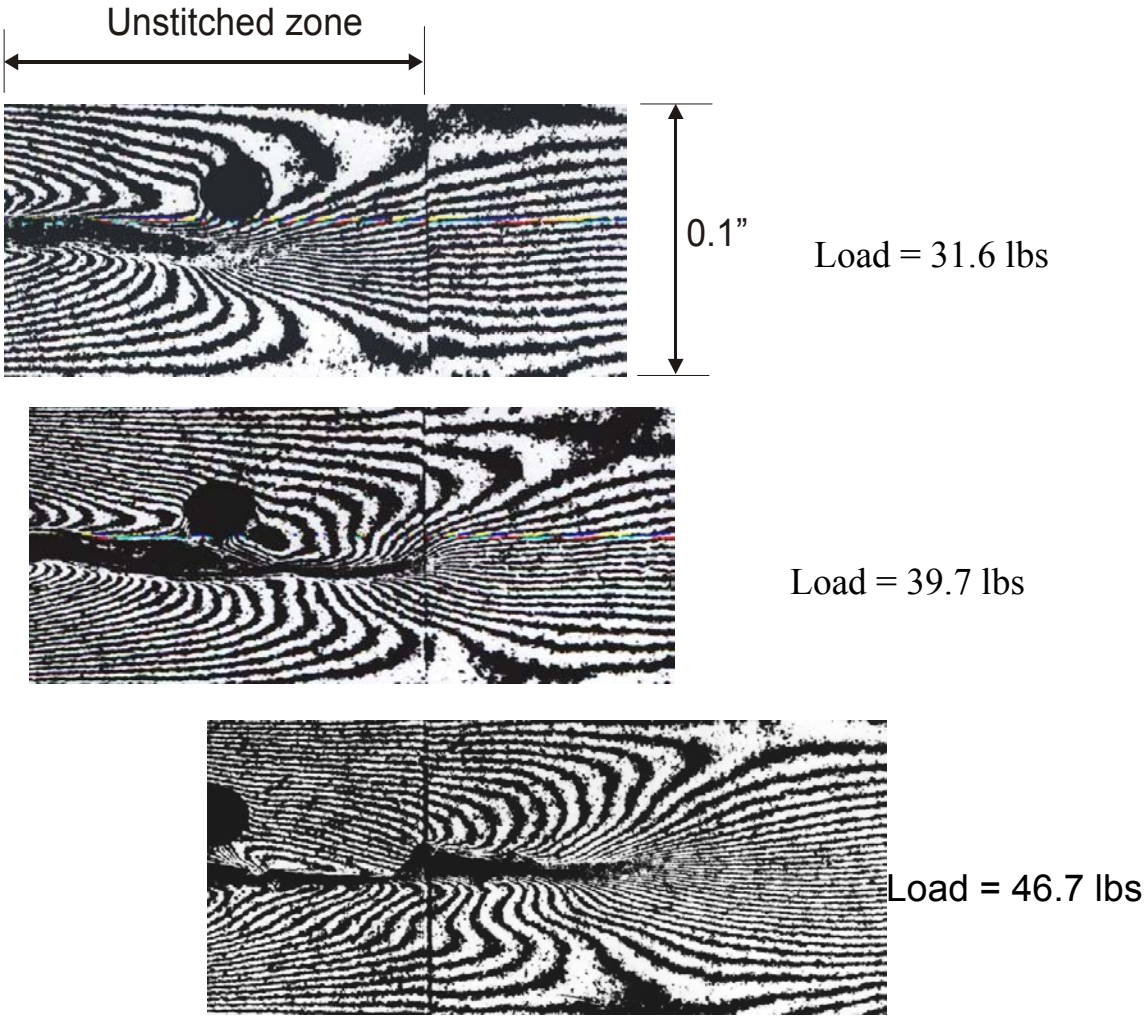

FIG. 8—*Moiré fringe patterns under various loading conditions for the cantilever beam setup.*

The crack surface displacements behind the crack tip of the three point bending setup are shown in Figs. 9 and10. It may be noted that the absolute values of the upper and lower surface displacements are equal for smaller loads (Fig. 9), but they differ significantly as the loads reach larger values (Fig. 10).

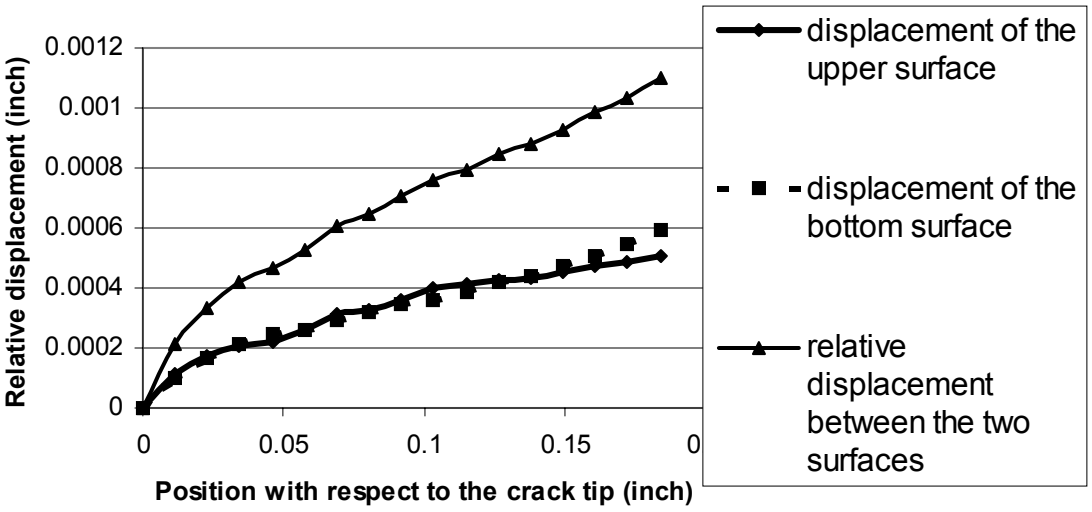

FIG. 9—*Relative crack surface displacement vs. distance from the crack tip in the three point bending setup when the load = 79.9 lbs (355 N). Stitch density = 40 stitches/in^2 (6.2 stitches/cm^2).*

This may be due to the asymmetry in the specimen about the delamination plane caused by stitching. One may note from Fig. 10 that it is difficult to obtain displacements very close to the crack tip (r < 0.02 in or 0.05 cm) for higher loads. This is because the strains in the vicinity of the crack tip reach much larger values causing very high fringe density, which is difficult to resolve. Nevertheless the crack-tip location can be accurately determined even for higher loads (Figs. 7 and 8).

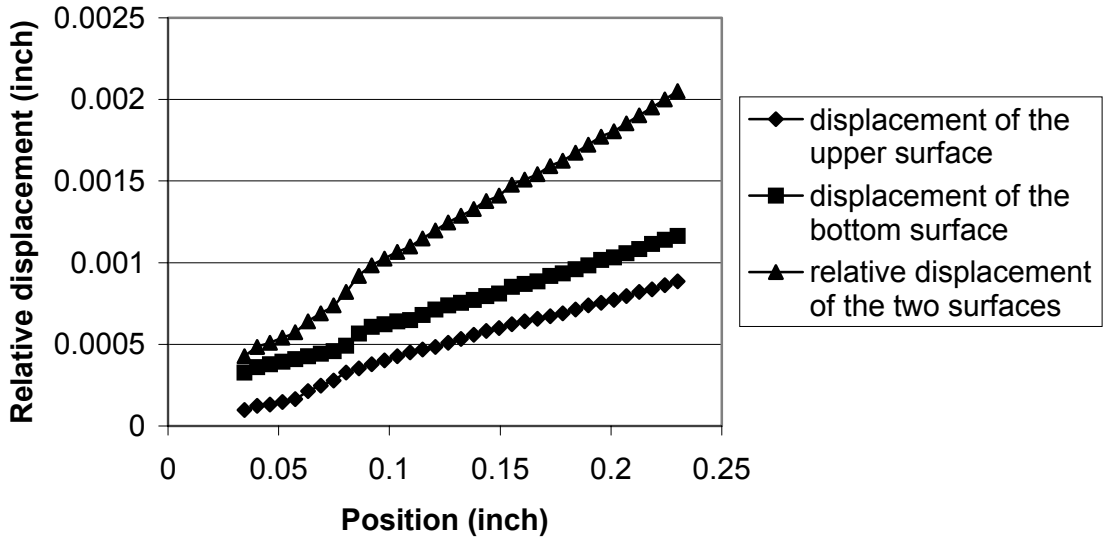

FIG. 10—*Relative crack surface displacement vs. distance from the crack tip in the three-point bending setup when the load = 189 lbs (841 N). Stitch density = 40 stitches/in^2 (6.2 stitches/cm^2).*

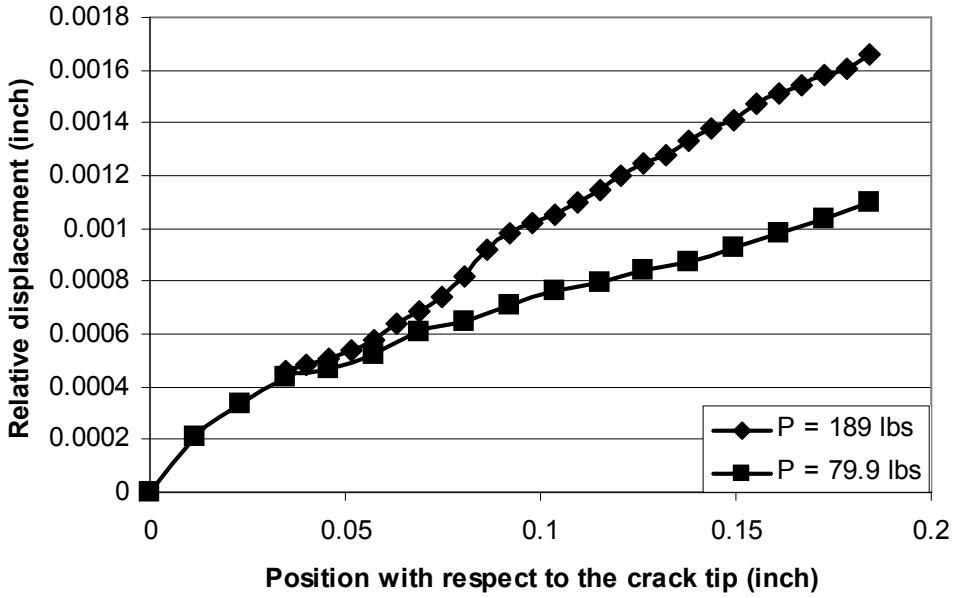

FIG. 11—*Comparison of relative crack surface displacements at two different loads. Stitch density = 40 stitches/in^2 (6.2 stitches/cm^2).*

Figure 11 shows that the relative displacements vary significantly with the loads when the positions are away from the crack tip. However, as one moves closer the crack tip, say less than 0.04 in (1mm), the relative displacement vs. crack extension curves for two loads (79.9 lbs and 189 lbs or 355 N and 841 N) coalesce (Fig. 11).

An expression for crack surface displacements u(r) can be obtained by substituting θ=+π or –π in the expression for u displacements in Eq. (3d). Then the relative crack surface displacements can be derived from Eq. (3d) as:

$$u(r,\pi) - u(r,-\pi) = \frac{K_{II}}{\bar{\mu}}\sqrt{\frac{2r}{\pi}} \tag{5}$$

where $\bar{\mu}$ depends on the orthotropic elastic constants. Then the stress intensity factor can be derived as

$$K_{II} = \underset{r\to 0}{Lim}\left(\bar{\mu}\sqrt{\frac{\pi}{2r}}\left(u(r,\pi) - u(r,-\pi)\right)\right) \tag{6}$$

Equation (6) can be written as

$$K_{II} = \underset{r\to 0}{Lim}\,\hat{K}_{II}(r) \tag{7}$$

where $\hat{K}_{II}(r)$ can be readily recognized by comparing Eqs. (6) and (7).

Alternatively one can evaluate the fracture toughness in terms of critical energy release rate G_{II} as

$$G_{IIc} = \lim_{r \to 0} \hat{G}_{II}(r) \tag{8}$$

where the term $\hat{G}_{II}(r)$ can be related to $\hat{K}_{II}(r)$ via Eq. (4):

$$\hat{G}_{II}(r) = \hat{K}_{II}^{\,2} \frac{a_{11}}{\sqrt{2}} \sqrt{\left(\frac{a_{22}}{a_{11}}\right)^{1/2} + \frac{2a_{12} + a_{66}}{2a_{11}}} \tag{9}$$

The value of $\hat{G}_{II}(r)$ was calculated for two different specimens and they are plotted in Fig. 12. The following are the material properties of the specimens used in both setups.

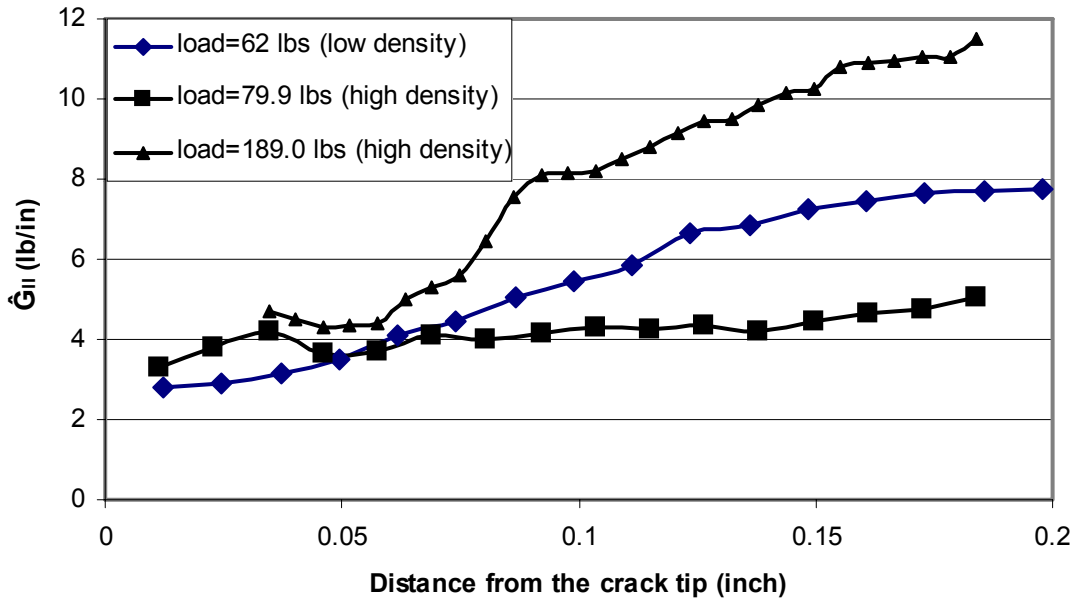

FIG. 12—*$\hat{G}_{II}(r)$ vs. r for various specimens at the instance of crack propagation. Low-density specimens had a stitch density of 20 stitches/in^2 (3.1 stitches/cm^2). High-density specimens had a stitch density of 40 stitches/in^2 (6.2 stitches/cm^2).*

$E_1 = 15.06 \times 10^6$ psi (103.8 Gpa), $E_2 = E_3 = 1.60 \times 10^6$ (11.0 Gpa) $\nu_{12} = 0.34$, $G_{12} = 0.80 \times 10^6$ psi (5.5 Gpa).

For plane strain, the roots of the characteristic equation (A5) of the Appendix can be obtained as

$$S_1 = 0.9980i, \quad S_2 = -0.9980i;$$
$$S_3 = 1.0020i, \quad S_4 = -1.0020i.$$

The stitch density and the load at which the calculations were made are indicated in Fig. 12. By extrapolating the curve to r=0, one can estimate the fracture toughness using Eq. (8). Since the crack has been under propagation at these load levels, the value of G_{II} estimated can be taken as the fracture toughness G_{IIC}. The values are given in Table 1.

TABLE 1—*Crack initiation loads and corresponding Mode II fracture toughness of two different stitched specimens.*

Specimen	Stitch density	Load	G_{IIC}
1	6.2 stitches/cm^2 (40 stitches/in^2)	79.9 lbs (355 N)	3.7 lb/in (648 N/m)
1	6.2 stitches/cm^2 (40 stitches/in^2)	189 lbs (841 N)	4.0 lb/in (700 N/m)
2	3.1 stitches/cm^2 (20 stitches/in^2)	62 lbs (276 N)	3.0 lb/in (525 N/m)

From the results one can note that the average G_{IIC} is about 3.6 lb/in (630 N/m), which is very close to the value of 3.4 lb/in (600 N/m) measured by Sharma and Sankar [5] for unstitched graphite/epoxy laminates. The results demonstrate that the crack tip actually propagates when the energy release rate reaches the value of fracture toughness of the material system. This fact will be useful in creating analytical and numerical models for Mode II delamination propagation of stitched composite laminates, *e.g.* [6].

As the crack propagates through the stitched zone, the crack tip stress field changes significantly. The crack surface displacements cannot be interpreted in the same manner as before. The moiré interferometry results for crack surface displacements u(r) obtained in this study for various stitched specimens would be of significant value in developing analytical and numerical models for delamination propagation in stitched specimens and in predicting the effective Mode II fracture toughness values presented in Fig. 6.

Conclusions

Moire interferometry was used to determine the displacement field in a stitched graphite/epoxy ENF specimen. From the moiré fringe patterns the relative crack surface displacements behind the crack tip were determined. The Mode II stress intensity factor was estimated using the linear elastic fracture mechanics theory for orthotropic materials. Another estimate of fracture toughness was obtained using the area method, which provides only an average value over a certain crack extension. The high sensitive moiré method was also used to determine the exact position of the crack tip in Mode II fracture tests. Stitching is found to increase the effective fracture toughness by factors of 2 to 3 for stitch densities of 20 and 40 stitches/in^2 (3.1 and 6.2 stitches/cm^2). However the crack seems to propagate, when the stress

intensity factor (energy release rate) as seen by the crack tip reaches the critical stress intensity factor (fracture toughness) for the parent (unstitched) material system.

Acknowledgements

This research was supported by the NSF Grant CMS-9732887 to the University of Florida. The authors are thankful to Dr. D. R. Ambur and Mr. D. M. McGowan of NASA Langley Research Center for the stitched composite specimens, and for their support and encouragement.

APPENDIX

The following equations for an orthotropic medium can be found in Ref. [14]. They are presented here for the convenience of readers as well as for the purpose of introducing the variables required for the discussion. The strain-stress relations for a plane orthotropic medium are given in Eq. (2). The governing differential equation for orthotropic materials can be derived in terms of the stress function *U(x y)* as

$$a_{22}\frac{\partial^4 U}{\partial x^4} - 2a_{26}\frac{\partial^4 U}{\partial x^3 \partial y} + (2a_{12} + a_{66})\frac{\partial^4 U}{\partial x^2 \partial y^2} - 2a_{16}\frac{\partial^4 U}{\partial x \partial y^3} + a_{11}\frac{\partial^4 U}{\partial y^4} = 0 \qquad \text{(A1)}$$

Defining the operators D_j (j = 1, 2, 3, 4) as

$$D_j = \frac{\partial}{\partial y} - \mu_j \frac{\partial}{\partial x} \qquad \text{(j = 1, 2, 3, 4)} \qquad \text{(A2)}$$

the governing equation in *U(x,y)* becomes

$$D_1 D_2 D_3 D_4 U(x,y) = 0 \qquad \text{(A3)}$$

The μ_j are the roots of the characteristic equation

$$a_{11}\mu_j^{\,4} - 2a_{16}\mu_j^{\,3} + (2a_{12} + a_{66})\mu_j^{\,2} - 2a_{26}\mu_j + a_{22} = 0 \qquad \text{(A4)}$$

The roots are either complex or purely imaginary and cannot be real and can be expressed as

$$\begin{aligned} s_1 &= \alpha_1 + i\beta_1, & s_2 &= \alpha_2 + i\beta_2, \\ s_3 &= \alpha_1 - i\beta_1, & s_4 &= \alpha_2 - i\beta_2 \end{aligned} \qquad \text{(A5)}$$

The stress function *U(x,y)* can be expressed in the form

$$U(x,y) = 2\mathrm{Re}[U_1(z_1) + U_2(z_2)] \qquad \text{(A6)}$$

Let new functions $\phi(z_1) = dU_1/dz_1$, $\psi(z_2) = dU_2/dz_2$

The stress and displacements components can be expressed as [14]

$$\sigma_x = 2\,\mathrm{Re}[s_1 2\phi'(z_1) + s_2{}^2\psi'(z_2)]$$
$$\sigma_y = 2\,\mathrm{Re}[\phi'(z_1) + \psi'(z_2)]$$
$$\tau_{xy} = -2\,\mathrm{Re}[s_1\phi'(z_1) + s_2\psi'(z_2)] \qquad \text{(A7)}$$
$$u_x = 2\,\mathrm{Re}[(a_{11}s_1{}^2 + a_{12} - a_{16}s_1)\phi(z_1) + (a_{11}s_2{}^2 + a_{12} - a_{16}s_2)\psi(z_2)]$$
$$u_y = 2\,\mathrm{Re}[(\frac{a_{12}s_1{}^2 + a_{22} - a_{26}s_1}{s_1})\phi(z_1) + (\frac{a_{12}s_2{}^2 + a_{22} - a_{26}s_2}{s_2})\psi(z_2)]$$

References

[1] Sharma, S.K. and B.V. Sankar (1995) "Effects of Through-the-Thickness Stitching on Impact and Interlaminar Fracture Properties of Textile Graphite/Epoxy Laminates", *NASA Contractor Report* 195042.

[2] Chen, L., B.V. Sankar, and P.G. Ifju (2001) "A novel double cantilever beam test for stitched composite laminates", *J. Composite Materials*, 35(13):1137-1149.

[3] Chen L., Sankar, B.V., Ifju P.G. (2002) "A new Mode I fracture test for composites with translaminar reinforcements", *Composites Science & Technology*, 62(10-11), 1407-1414.

[4] Sharma, S.K. and B.V. Sankar (1997) "Mode II Delamination Toughness of Stitched Graphite/Epoxy Textile Composites", *Composites Science and Technology*, 57(7):729-737.

[5] Sharma, S.K. and B.V. Sankar (1997) "Effect of Stitching on Impact and Interlaminar Properties of Graphite/Epoxy Laminates", *J. Thermoplastic Composite Materials*, 10(3):241-253.

[6] Sankar, B.V. and Sonik, V. (1995) "Modeling End Notched Flexure Test of Stitched Composite Laminates" *Proceedings of the American Society for Composites,* Tenth Technical Conference, Technomic Publications, Lancaster, Pennsylvania, pp. 172-181.

[7] Jain, L.K and Mai, Y. (1994b) "Analysis of stitched laminated ENF specimens for interlaminar mode II fracture toughness".

[8] Massabo, R. and Cox, B.N. (1996) "Concepts for bridged Mode II delamination cracks", *Materials Science report, Rockwell Science Center*.

[9] Ogo, Y. (1987) "The effect of stitching on in-plane and interlaminar properties of carbon-epoxy fabric laminates", *CCM Report Number 87-17, Center for Composite Materials*, University of Delaware, Newark, May 1987.

[10] Dickinson, L.C., G. L. Farley, and M. K. Hinders "Translaminar Reinforced Composites: A Review" *Journal of Composites Technology & Research*, JCTRER, Vol. 21, No. 1, 1999, pp. 3-15.

[11] Massabo, R. D.R, Mumm and B.N. Cox "Characterizing mode II delamination cracks in stitched composites", *International Journal of Fracture* 92: 1-38, 1998.

[12] Sankar, B.V. (1991) "A Finite Element for Modeling Delaminations in Composite Beams", *Computers & Structures*, 38(2): 239-246.

[13] Post, D., B. Han and P. Ifju (1994), High sensitivity Moiré: Experimental Stress Analysis for Materials, Mechanical Engineering Series, Springer-Verlag, New York, NY.

[14] Sih, G. C. and H. Liebowitz. (1968) “Mathematical Theories of Brittle Fracture” Fracture an Advance Treatise (Volume II), Ed. H. Liebowitz, Academic Press, New York.